Detection, Estimation, and Modulation Theory, Part III: Radar–Sonar Signal Processing and Gaussian Signals in Noise. Harry L. Van Trees

ISBNs: 0-471-10793-X (Paperback); 0-471-22109-0 (Electronic)

13

Doubly-Spread Targets and Channels

In this chapter, we generalize our model to include targets that are doubly-spread. There are several areas in which this type of target (or channel) is encountered.

A simple example of the first area arises in sonar systems. When an acoustic pulse is transmitted into the ocean, energy is returned from a large number of objects distributed throughout the ocean. If a submarine or ship is present, it also reflects the pulse. The latter reflection provides the information bearing signal and the scattered returns from other objects constitute the interference. The reflectors that cause the interference have various velocities and reflective cross-sections. In a reasonable model we assign a random amplitude and phase to each reflection. The location of the scatterers can be modeled as a spatial Poisson process whose mean-value function governs the average density. The velocity of the scatterers can be modeled by assigning a range-dependent probability density for the velocity of each scatterer. If we use this approach and assume a large number of scatterers, the result is a reverberation return that is a sample function from a Gaussian random process. The Poisson model has a great deal of physical appeal. It is developed quantitatively in [1]–[4]. In the next section we obtain the same Gaussian result in a less physical, but computationally simpler, manner. The first distinguishing feature of this type of problem is that the *spread* target corresponds to an *unwanted* return that we want to eliminate. The second feature is that the target is "soft" (i.e., its physical structure is not fixed).

A second area in which doubly-spread targets occur is one in which the details of the target are the quantities of interest. This area is encountered in mapping radars (e.g., ground mapping from airplanes or satellites; moon or planet mapping from the ground). Here we try to measure the detailed structure of the scattered return. We shall find that the return

from the different segments of the target acts as a source of interference in the measurement problem. A second feature of this area is that the target is "hard" (i.e., its physical structure is fixed).

A third area of interest arises when we try to communicate over dispersive fluctuating channels (e.g., ionospheric and tropospheric channels, underwater acoustic channels, the orbiting dipole channel, local battlefield communication using chaff clouds). Here the return from the scatterers corresponds to the wanted signal, and the interference is some additive noise process. In addition, we see that the channel is "soft" (i.e., its physical structure changes).

The fourth area is radar astronomy. Here we want to measure the range and velocity of a rotating target that has an appreciable depth. Once again, the return from the spread target contains the desired information and the interference is an additive noise process. In this case, the target is "hard" and has a surface that is rough compared to the carrier wavelength.

We see that the areas of interest can be divided into two groups. In the first, the return from the spread target (or channel) is a source of interference. In the second, the return from the spread target (or channel) contains the desired information. In this chapter we study representative problems from the two groups.

In Section 13.1, we develop a simple model for a doubly-spread target and discuss its effect on the transmitted signal. We then use this model to study a sequence of problems.

In Section 13.2, we study the continuous resolution problem in active radar and sonar systems. This discussion is an extension of the discrete resolution problem in Section 10.5. The desired target is a slowly fluctuating point target. The interference is modeled as a continuum of reflectors, using the doubly-spread target model of Section 13.1. We then study receiver design and signal design for this type of environment. This problem, which is referred to as the reverberation problem in the sonar field and the clutter problem in the radar field, completes the discussion that we began in Chapter 10.

In Section 13.3, we study the detection of the return from a doubly-spread target in the presence of noise. This problem is just one of detecting a complex Gaussian process in complex white noise, which we first encountered in Section 11.2. However, the covariance function of the signal process is quite complicated, and it is appreciably harder to solve the problem.

In Section 13.4, we study the parameter-estimation problem briefly. Specifically, we consider the problem of estimating the amplitude of a doubly-spread target and the problem of estimating the mean range and mean Doppler of a doubly-spread target.

The major sections of the Chapter, 13.2 and 13.3, are almost independent. The reader who is interested only in communications can proceed directly from Section 13.1 to 13.3. Section 13.4 can also be read after Section 13.1. The results of the chapter are summarized in Section 13.5.

13.1 MODEL FOR A DOUBLY-SPREAD TARGET

Our model for a fluctuating range-spread target is a simple combination of the models in Chapters 11 and 12.

13.1.1 Basic Model

To illustrate the ideas involved, we consider the rotating sphere shown in Fig. 13.1. The surface of the sphere is rough compared to the wavelength of the carrier. We transmit a signal whose complex envelope is $\tilde{f}(t)$ and examine the reflected signal from the range interval $(\lambda, \lambda + d\lambda)$. The signal is the superposition of the number of reflections with random phases and can be modeled as a Rayleigh random variable. Since the orientation and composition of the reflectors that contribute to the returned signal change as functions of time (see Fig. 13.1*b* and *c*), we must model the reflection as a random process. Thus,

$$\tilde{s}(t, \lambda) = \sqrt{E_t}\tilde{f}(t - \lambda)\tilde{b}\left(t - \frac{\lambda}{2}, \lambda\right) d\lambda, \tag{1}$$

where $\tilde{b}(t, \lambda)$ is a complex Gaussian process whose independent variables are *both* time and space. The return from the entire target is a superposition of the returns from the incremental intervals. The complex envelope,

$$\tilde{s}(t) = \int_{-\infty}^{\infty} \sqrt{E_t}\tilde{f}(t - \lambda)\tilde{b}\left(t - \frac{\lambda}{2}, \lambda\right) d\lambda, \tag{2}$$

is a sample function from a zero-mean complex Gaussian process. It can be characterized by the covariance function

$$\begin{aligned}
\tilde{K}_{\tilde{s}}(t, u) &\triangleq E[\tilde{s}(t)\tilde{s}^*(u)] \\
&= E\left\{\int_{-\infty}^{\infty}\int E_t\tilde{f}(t - \lambda)\tilde{f}^*(u - \lambda_1)\tilde{b}\left(t - \frac{\lambda}{2}, \lambda\right)\tilde{b}^*\left(u - \frac{\lambda_1}{2}, \lambda_1\right) d\lambda\, d\lambda_1\right\} \\
&= E_t\int_{-\infty}^{\infty}\int \tilde{f}(t - \lambda)\left\{E\left[\tilde{b}\left(t - \frac{\lambda}{2}, \lambda\right)\tilde{b}^*\left(u - \frac{\lambda_1}{2}, \lambda_1\right)\right]\right\} \\
&\quad \times \tilde{f}^*(u - \lambda_1)\, d\lambda\, d\lambda_1.
\end{aligned} \tag{3}$$

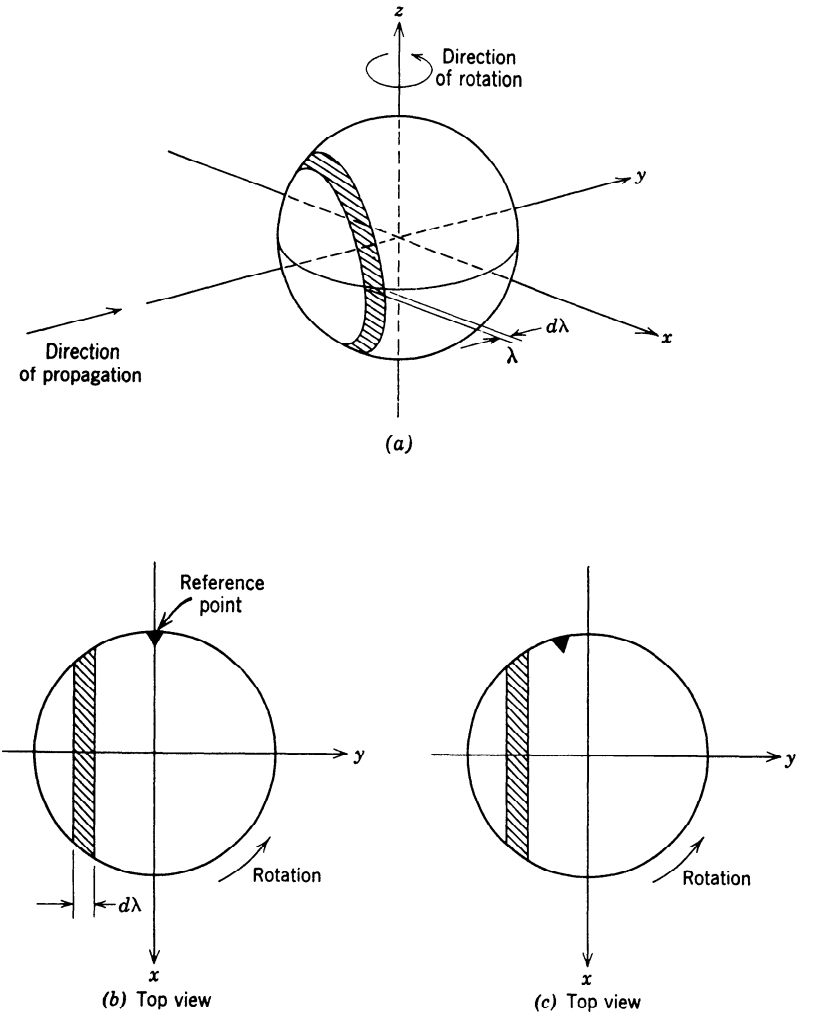

Fig. 13.1 Rough rotating sphere.

The statistical characteristics of the target specify the term in braces. We make two assumptions:

1. The returns from different intervals are statistically independent. (This corresponds to the model in Chapter 12.)
2. The return from each interval is a sample function of a *stationary*, zero-mean complex Gaussian random process. (This corresponds to the model in Chapter 11.)

Using these two assumptions, we can write

$$E[\tilde{b}(t, \lambda)\tilde{b}^*(u, \lambda_1)] = \tilde{K}_{DR}(t - u, \lambda)\delta(\lambda - \lambda_1). \tag{4}$$

The function $K_{DR}(\tau, \lambda)$ is a two-variable function that depends on the reflective properties of the target. Using (4) in (3) gives

$$\boxed{\tilde{K}_{\tilde{g}}(t, u) = E_t \int_{-\infty}^{\infty} \tilde{f}(t - \lambda)\tilde{K}_{DR}(t - u, \lambda)\tilde{f}^*(u - \lambda)\, d\lambda} \tag{5}$$

as a complete characterization of the returned signal process.

Just as in the singly-spread case, it is convenient to introduce a *scattering function*, which is defined as

$$\boxed{\tilde{S}_{DR}\{f, \lambda\} = \int_{-\infty}^{\infty} e^{-j2\pi f\tau}\tilde{K}_{DR}(\tau, \lambda)\, d\tau.} \tag{6}$$

Physically, $\tilde{S}_{DR}\{f, \lambda\}$ represents the spectrum of the process $\tilde{b}(t, \lambda)$. It is a *real, non-negative* function of f and λ. The scattering function of a rough rotating sphere is shown in Fig. 13.2. (This result is derived in [5].) Two other scattering functions that we shall use as models are shown in Figs 13.3 and 13.4. In Fig. 13.3,

$$\tilde{S}_{DR}\{f, \lambda\} = \frac{2ck(\lambda)}{(2\pi f)^2 + k^2(\lambda)}, \qquad -\infty < f < \infty, \qquad 0 < \lambda < L. \tag{7}$$

At each value of λ, the spectrum is a first-order Butterworth process, but the pole location is a function of λ. This is an approximate model for some communications channels. In Fig. 13.4,

$$\tilde{S}_{DR}\{f, \lambda\} = \frac{\sigma_b^2}{\pi\sigma_R\sigma_D} \exp\left[-\frac{f^2}{2\sigma_D^2} - \frac{\lambda^2}{2\sigma_R^2}\right], \qquad -\infty < f, \lambda < \infty. \tag{8}$$

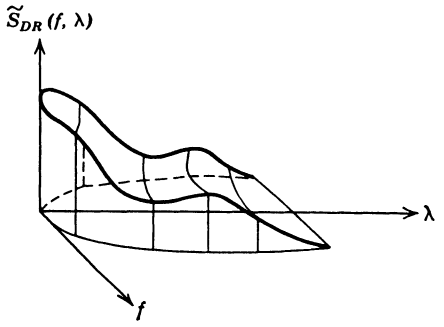

Fig. 13.2 Scattering function of a rough sphere [from [5]].

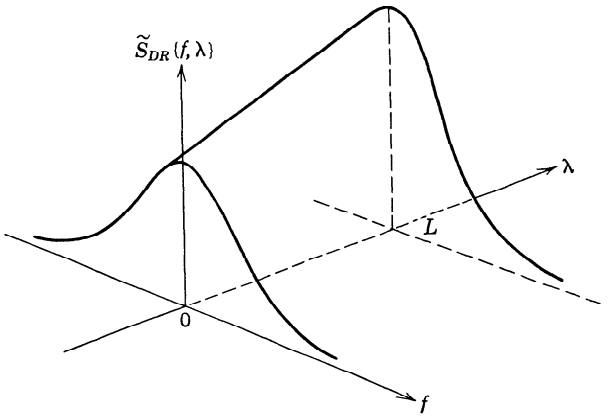

Fig. 13.3 A scattering function example.

The doubly Gaussian scattering function never occurs exactly, but is a useful approximation in many situations. Other examples of scattering functions are given on pages 35–39 of [37].

We can also write (5) using the scattering function as

$$\tilde{K}_{\tilde{s}}(t, u) = E_t \int_{-\infty}^{\infty} \tilde{f}(t - \lambda) \tilde{S}_{DR}\{f, \lambda\} \tilde{f}^*(u - \lambda) e^{j2\pi f(t-u)}\, df\, d\lambda. \tag{9}$$

There are several properties of the model that will be useful, and we include them at this point.

Property 1. Received Energy. The *average* value of the received energy is

$$E[E_r] \triangleq \bar{E}_r = \int_{-\infty}^{\infty} \tilde{K}_{\tilde{s}}(t, t)\, dt. \tag{10}$$

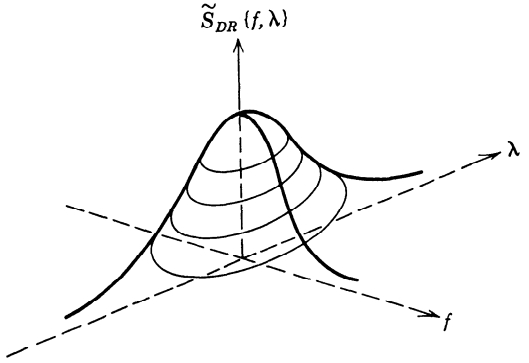

Fig. 13.4 A doubly-Gaussian scattering function (drawn for $\sigma_D < \sigma_R$).

Using (9) gives

$$\bar{E}_r = E_t \int_{-\infty}^{\infty} df \int_{-\infty}^{\infty} d\lambda \int_{-\infty}^{\infty} dt \, |\tilde{f}(t - \lambda)|^2 \, \tilde{S}_{DR}\{f, \lambda\}. \tag{11}$$

The integral with respect to t equals 1 for all λ. Thus,

$$\bar{E}_r = E_t \iint_{-\infty}^{\infty} \tilde{S}_{DR}\{f, \lambda\} \, df \, d\lambda. \tag{12}$$

To be consistent with our earlier models, we assume that

$$\iint_{-\infty}^{\infty} \tilde{S}_{DR}\{f, \lambda\} \, df \, d\lambda = 2\sigma_b^2. \tag{13}$$

We see that the double integral of the scattering function is the ratio of the expected value of the received energy to the transmitted energy. Notice that the received energy is not a function of the signal shape.

Property 2. When a scattering function is concentrated in one region of the f, λ plane, we can characterize it grossly in terms of its moments. The mean delay is

$$m_R \triangleq \frac{1}{2\sigma_b^2} \int_{-\infty}^{\infty} d\lambda \, \lambda \int_{-\infty}^{\infty} df \, \tilde{S}_{DR}\{f, \lambda\}. \tag{14}$$

The mean-square delay spread is

$$\sigma_R^2 \triangleq \frac{1}{2\sigma_b^2} \int_{-\infty}^{\infty} d\lambda \, \lambda^2 \int_{-\infty}^{\infty} df \, \tilde{S}_{DR}\{f, \lambda\} - m_R^2. \tag{15}$$

The mean Doppler shift is

$$m_D \triangleq \frac{1}{2\sigma_b^2} \int_{-\infty}^{\infty} df f \int_{-\infty}^{\infty} d\lambda \, \tilde{S}_{DR}\{f, \lambda\}. \tag{16}$$

The mean-square Doppler spread is

$$\sigma_D^2 \triangleq \frac{1}{2\sigma_b^2} \int_{-\infty}^{\infty} df f^2 \int_{-\infty}^{\infty} d\lambda \, \tilde{S}_{DR}\{f, \lambda\} - m_D^2. \tag{17}$$

The skewness is measured by

$$\rho_{DR} = \frac{\overline{f\lambda} - m_R m_D}{\sigma_D \sigma_R}, \tag{18}$$

where

$$\overline{f\lambda} \triangleq \frac{1}{2\sigma_b^2} \int_{-\infty}^{\infty} df f \int_{-\infty}^{\infty} d\lambda \, \lambda \tilde{S}_{DR}\{f, \lambda\}. \tag{19}$$

In contrast with these mean-square measures, we frequently encounter scattering functions that are strictly bandlimited to B cps and/or are strictly limited in length to L seconds. In these cases the absolute measure is usually more useful.

Property 3. Alternative Characterizations. We saw that two functions that characterized the target were $\tilde{K}_{DR}(\tau, \lambda)$ and $\tilde{S}_{DR}\{f, \lambda\}$. Two other functions obtained by Fourier-transforming with respect to λ are

$$\tilde{P}_{DR}\{f, v\} \triangleq \int_{-\infty}^{\infty} d\lambda \, e^{-j2\pi v\lambda} \tilde{S}_{DR}\{f, \lambda\} \tag{20}$$

and

$$\tilde{R}_{DR}\{\tau, v\} \triangleq \int_{-\infty}^{\infty} d\lambda \, e^{-j2\pi v\lambda} \tilde{K}_{DR}(\tau, \lambda). \tag{21}$$

Notice the sign convention in the Fourier transform. Transforming from t to f and from λ to v, we use the minus sign in the exponent. (Remember that both v and f are frequency variables.) These functions are summarized in Fig. 13.5. The significance of the various variables should be emphasized. We can consider the f, τ pair and the λ, v pair separately.

1. A "short" target is narrow on the λ-axis and therefore is wide on the v-axis.
2. A point target is an impulse on the λ-axis and therefore is a constant for all values of v.

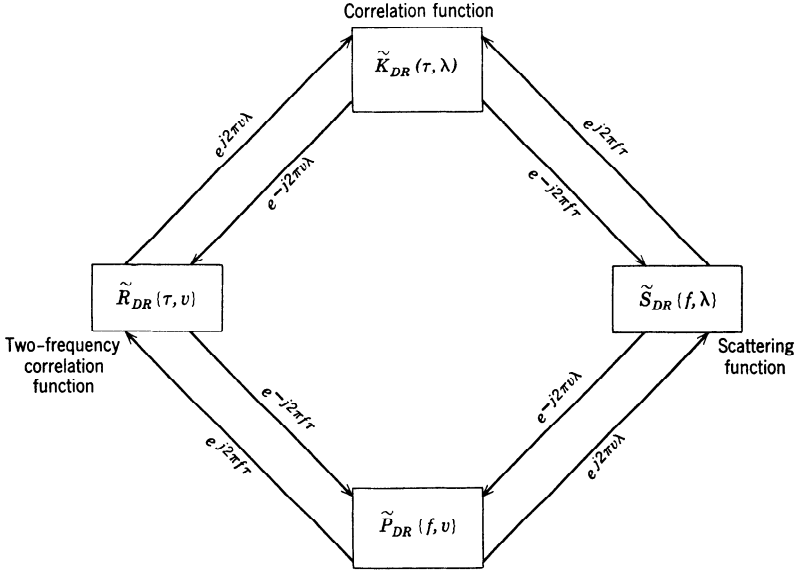

Fig. 13.5 Target and channel characterizations.

3. An infinite-depth target is constant along the λ-axis and therefore is an impulse on the v-axis.

4. A slowly fluctuating target is narrow on the f-axis and therefore is wide on the τ-axis.

5. A fixed target is an impulse on the f-axis and therefore is a constant on the τ-axis.

6. A rapidly fluctuating target is wide on the f-axis and impulsive on the τ-axis.

The advantage of having several characterizations is that one is frequently easier to use than the others. We shall encounter several examples at various points in the chapter. Notice that, except for a $2\sigma_b^2$ factor, the scattering function, $\tilde{S}_{DR}\{f, \lambda\}$, has all of the properties of a joint probability density. Thus, $\tilde{R}_{DR}\{\tau, v\}$ is analogous to a joint characteristic function.

Property 4. Degenerate Targets. Both singly-spread target models can be viewed as limiting cases of a doubly-spread target. Repeating (5), we have

$$\tilde{K}_{\tilde{s}}(t, u) = E_t \int_{-\infty}^{\infty} \tilde{f}(t - \lambda)\tilde{K}_{DR}(t - u, \lambda)\tilde{f}^*(u - \lambda)\, d\lambda. \tag{22}$$

To obtain the point target model, we assume that the length of the target along the λ-axis is much less than the reciprocal of the signal bandwidth; that is,

$$L \ll \frac{1}{W}. \tag{23}\dagger$$

Then we can treat $\tilde{f}(t - \lambda)$ as a constant function of λ over the range where $\tilde{K}_{DR}(t - u, \lambda)$ is nonzero. Consequently we can approximate $\tilde{K}_{DR}(t - u, \lambda)$ as

$$\tilde{K}_{DR}(t - u, \lambda) \simeq \tilde{K}_D(t - u)\delta(\lambda - \bar{\lambda}). \tag{24}$$

Using (24) in (22) gives

$$\tilde{K}_{\tilde{s}}(t, u) = E_t \tilde{f}(t - \bar{\lambda})\tilde{K}_D(t - u)\tilde{f}^*(u - \bar{\lambda}), \tag{25}$$

which is (11.20). If (23) is satisfied, we have a fluctuating point target whose fading is *not* frequency-selective.

† In (23), (27), and (30) we use B, L, W, and T in an intuitive manner. For a particular signal and target, the statements can be made more precise.

To obtain the nonfluctuating model, we start with the expression in (9),

$$\tilde{K}_{\tilde{s}}(t, u) = E_t \int\int_{-\infty}^{\infty} \tilde{f}(t - \lambda)\tilde{S}_{DR}\{f, \lambda\}\tilde{f}^*(u - \lambda)e^{j2\pi f(t-u)}\, df\, d\lambda. \quad (26)$$

If

$$B \ll \frac{1}{T}, \quad (27)$$

then we can use the approximation

$$\tilde{S}_{DR}\{f, \lambda\} \simeq \tilde{S}_R\{\lambda\}\delta\{f - \bar{f}\}. \quad (28)$$

Using (28) in (26), we obtain

$$\tilde{K}_{\tilde{s}}(t, u) = E_t \int_{-\infty}^{\infty} \tilde{f}(t - \lambda)e^{j2\pi\bar{f}t}\tilde{S}_R\{\lambda\}\tilde{f}^*(u - \lambda)e^{-j2\pi\bar{f}u}\, d\lambda, \quad (29)$$

which corresponds to the return from a nonfluctuating range-spread target moving at a constant velocity. If (27) is satisfied, the fading is *not* time-selective.

In order to have an undistorted returned signal (i.e., fading that is flat in both time and frequency), both (23) and (27) must be satisfied. Combining them, we have

$$BL \ll \frac{1}{WT}. \quad (30)$$

Because

$$WT > 1 \quad (31)$$

for all signals, the condition in (30) can only be satisfied for $BL < 1$.

We refer to targets (or channels) for which

$$BL < 1 \quad (32)$$

as *underspread* targets (or channels). If

$$BL > 1, \quad (33)$$

we say that the target (or channel) is *overspread.* We shall look at further implications of the BL product as we proceed through the chapter. Our present discussion shows that only underspread targets that satisfy (30) will ever degenerate into slowly fluctuating point targets for certain signals.

It is worthwhile recalling that the Doppler spread depends on both the target velocity spread and the carrier frequency (see (9.24)). Thus the BL product for a particular target will depend on the carrier frequency.

Up to this point we have characterized the reflection process $\tilde{b}(t, \lambda)$ in terms of its covariance function or spectrum. It is frequently convenient

to use a differential-equation model of the channel process. We develop this model in the next section.

13.1.2 Differential-Equation Model for a Doubly-Spread Target (or Channel)†

In our model for a doubly-spread target we have assumed that th returns from different range elements are statistically independent. The covariance function of the reflection process is

$$E[\tilde{b}(t, \lambda)\tilde{b}^*(u, \lambda')] = \tilde{K}_{DR}(t - u, \lambda)\delta(\lambda - \lambda'). \tag{34}$$

In many cases of interest the Fourier transform of $\tilde{K}_{DR}(t - u)$ is a rational function of f. In these cases we can derive a state-variable model for the doubly-spread channel. Notice that (34) implies that there is no relationship between the target processes at different values of λ. Thus we can treat the target process at any point (say λ_1) as a random process with a single independent variable t. Then the state representations developed in Section I–6.3.3 are immediately applicable. The first new feature is that the state equations will contain λ as a parameter. Other new features will be encountered as we proceed through the development.

Since the output of the channel is given by

$$\tilde{s}(t) = \int_{-\infty}^{\infty} \sqrt{E_t}\tilde{f}(t - \lambda)\tilde{b}\left(t - \frac{\lambda}{2}, \lambda\right) d\lambda, \tag{35}$$

it is convenient to define a new process

$$\tilde{b}_x(t, \lambda) \triangleq \tilde{b}\left(t - \frac{\lambda}{2}, \lambda\right). \tag{36}$$

Notice that $\tilde{b}_x(t, \lambda)$ is a zero-mean complex Gaussian process whose covariance function is

$$\begin{aligned} E[\tilde{b}_x(t, \lambda)\tilde{b}_x^*(u, \lambda')] &= E\left[\tilde{b}\left(t - \frac{\lambda}{2}, \lambda\right)\tilde{b}^*\left(u - \frac{\lambda'}{2}, \lambda'\right)\right] \\ &= \tilde{K}_{DR}(t - u, \lambda)\,\delta(\lambda - \lambda'). \end{aligned} \tag{37}$$

We have modeled the channel reflection process as a random process that depends on both time and space. We now want to characterize the time dependence by a state-variable representation. The spatial dependence is included by making the state representation a function of the

† This channel model was developed by R. Kurth in his doctoral thesis [7]. It is used primarily in sections 13.2.2 and 13.3. One can defer reading this section until that point.

spatial variable λ. The representation that we need to describe a doubly-spread channel incorporates the spatial dependence in a straightforward manner.

We denote the state vector of $\tilde{b}_x(t, \lambda)$ as $\tilde{\mathbf{x}}(t, \lambda)$. The state equation is

$$\boxed{\frac{\partial \tilde{\mathbf{x}}(t, \lambda)}{\partial t} = \tilde{\mathbf{F}}(\lambda)\tilde{\mathbf{x}}(t, \lambda) + \tilde{\mathbf{G}}(\lambda)\tilde{u}(t, \lambda), \qquad t \geq T_i,} \tag{38}$$

where

$$\boxed{E[\tilde{u}(t, \lambda)\tilde{u}^*(\tau, \lambda')] = \tilde{Q}(\lambda)\,\delta(t - \tau)\,\delta(\lambda - \lambda').} \tag{39}$$

The initial covariance of the state vector is

$$\boxed{E[\tilde{\mathbf{x}}(T_i, \lambda)\tilde{\mathbf{x}}^\dagger(T_i, \lambda')] = \tilde{\mathbf{P}}_0(\lambda)\,\delta(\lambda - \lambda').} \tag{40}$$

The channel process is

$$\tilde{b}_x(t, \lambda) = \tilde{\mathbf{C}}(\lambda)\tilde{\mathbf{x}}(t, \lambda). \tag{41}$$

Notice that there is no coupling between the different values of λ in the description. The state equation is written as a partial differential equation, but it is actually just an ordinary differential equation containing λ as a parameter. Because of this parametric dependence, we can write a covariance equation easily. We define

$$\begin{aligned}\tilde{\mathbf{K}}_{\tilde{\mathbf{x}}}(t, t':\lambda, \lambda') &\triangleq E[\tilde{\mathbf{x}}(t, \lambda)\tilde{\mathbf{x}}^\dagger(t', \lambda')] \\ &= \tilde{\mathbf{K}}_{\tilde{\mathbf{x}}}(t, t':\lambda)\,\delta(\lambda - \lambda').\end{aligned} \tag{42}$$

As before, $\tilde{\mathbf{K}}_{\tilde{\mathbf{x}}}(t, t':\lambda)$ can be related to $\tilde{\mathbf{K}}_{\tilde{\mathbf{x}}}(t, t:\lambda)$ by the relation

$$\tilde{\mathbf{K}}_{\tilde{\mathbf{x}}}(t, t':\lambda) = \begin{cases}\tilde{\boldsymbol{\theta}}(t - t':\lambda)\tilde{\mathbf{K}}_{\tilde{\mathbf{x}}}(t', t:\lambda), & t \geq t', \\ \tilde{\mathbf{K}}_{\tilde{\mathbf{x}}}(t, t)\tilde{\boldsymbol{\theta}}^\dagger(t' - t:\lambda), & t \leq t',\end{cases} \tag{43}$$

where $\tilde{\boldsymbol{\theta}}(t:\lambda)$ is the transition matrix and is the solution to

$$\frac{\partial \tilde{\boldsymbol{\theta}}(t:\lambda)}{\partial t} = \tilde{\mathbf{F}}(\lambda)\tilde{\boldsymbol{\theta}}(t:\lambda), \tag{44}$$

with the initial condition

$$\tilde{\boldsymbol{\theta}}(0, \lambda) = \mathbf{I}. \tag{45}$$

Notice that the transition matrix has a single time argument, because $\tilde{\mathbf{F}}(\lambda)$ and $\tilde{\mathbf{G}}(\lambda)$ are not functions of time.

Since we have assumed that the channel process is stationary, $\tilde{\mathbf{K}}_{\tilde{\mathbf{x}}}(t, t:\lambda)$ is not a function of time. Thus we can write

$$\bar{\mathbf{K}}_{\tilde{\mathbf{x}}}(\lambda) \triangleq \tilde{\mathbf{K}}_{\tilde{\mathbf{x}}}(t, t:\lambda), \qquad t \geq T_i. \tag{46}$$

The matrix $\tilde{\mathbf{K}}_{\tilde{\mathbf{x}}}(\lambda)$ is just the solution to

$$\mathbf{0} = \tilde{\mathbf{F}}(\lambda)\tilde{\mathbf{K}}_{\tilde{\mathbf{x}}}(\lambda) + \tilde{\mathbf{K}}_{\tilde{\mathbf{x}}}(\lambda)\tilde{\mathbf{F}}^{\dagger}(\lambda) + \tilde{\mathbf{G}}(\lambda)\tilde{\mathbf{Q}}(\lambda)\tilde{\mathbf{G}}^{\dagger}(\lambda) \tag{47}$$

[see (I-6.333*a*)]. Notice that the stationarity assumption requires

$$\tilde{\mathbf{P}}_0(\lambda) = \tilde{\mathbf{K}}_{\tilde{\mathbf{x}}}(\lambda). \tag{48}$$

The channel covariance function is obtained by using (41) and (42) in (37) to obtain

$$\boxed{\tilde{K}_{D\tilde{R}}(\tau, \lambda) = \tilde{\mathbf{C}}(\lambda)\tilde{\mathbf{K}}_{\tilde{\mathbf{x}}}(\tau, \lambda)\tilde{\mathbf{C}}^{\dagger}(\lambda).} \tag{49}$$

Once again we emphasize that all the results are ordinary state-variable results with a parametric dependence on λ. To complete our model, we must describe the observed signal process. Using (36) in (35) gives

$$\tilde{s}(t) = \int_{-\infty}^{\infty} \sqrt{\bar{E}_t}\tilde{f}(t - \lambda)\tilde{b}_x(t, \lambda)\, d\lambda. \tag{50}$$

Using (41) in (50), we have

$$\boxed{\tilde{s}(t) = \int_{-\infty}^{\infty} \sqrt{\bar{E}_t}\tilde{f}(t - \lambda)\tilde{\mathbf{C}}(\lambda)\tilde{\mathbf{x}}(t, \lambda)\, d\lambda.} \tag{51}$$

We see that (51) contains an integration over the spatial variable λ. This spatial functional is the new feature of the problem and will require extension of our earlier state-variable theory. Notice that it is a *linear* functional and is analogous to the modulation matrix in Section 6.6.3. It is sometimes convenient to rewrite (51) as

$$\boxed{\tilde{s}(t) = \tilde{s}(t:\tilde{\mathbf{x}}(t, \lambda)).} \tag{52}$$

This completes our differential equation model of the doubly-spread channel. To illustrate the techniques involved, we consider an example.

Example [7]. We consider a complex first-order state equation

$$\frac{\partial \tilde{x}(t, \lambda)}{\partial t} = -\tilde{k}(\lambda)\tilde{x}(t, \lambda) + \tilde{u}(t, \lambda), \tag{53}$$

and

$$\tilde{b}_x(t, \lambda) = c\tilde{x}(t, \lambda). \tag{54}$$

These equations correspond to (38)–(41) with

$$\tilde{\mathbf{F}}(\lambda) = -\tilde{k}(\lambda) = -k_r(\lambda) - jk_i(\lambda), \tag{55}$$

$$\tilde{\mathbf{G}}(\lambda) = 1, \tag{56}$$

and

$$\tilde{C}(\lambda) = c. \tag{57}$$

We assume

$$\tilde{Q}(\lambda) \geq 0 \tag{58}$$

and

$$k_r(\lambda) > 0. \tag{59}$$

From (44) and (45), we have

$$\tilde{\theta}(\tau, \lambda) = \exp\left[-k_r(\lambda)\,|\tau| - jk_i(\lambda)\tau\right], \tag{60}$$

and from (47),

$$\tilde{K}_{\tilde{x}}(\lambda) = \frac{\tilde{Q}(\lambda)}{2k_r(\lambda)}. \tag{61}$$

Using (60) and (61) in (43) and the result in (49) gives the channel covariance function as

$$\tilde{K}_{DR}(\tau, \lambda) = \frac{c^2\tilde{Q}(\lambda)}{2k_r(\lambda)} \exp\left[-k_r(\lambda)\,|\tau| - jk_i(\lambda)\tau\right]. \tag{62}$$

Transforming gives the channel-scattering function as

$$\tilde{S}_{DR}\{f, \lambda\} = \frac{c^2\tilde{Q}(\lambda)}{(2\pi f + k_i(\lambda))^2 + k_r^2(\lambda)}. \tag{63}$$

Notice that

$$\int_{-\infty}^{\infty}\int S_{DR}\{f, \lambda\}\, df\, d\lambda = c^2 \int_{-\infty}^{\infty} \frac{\tilde{Q}(\lambda)}{2k_r(\lambda)}\, d\lambda \triangleq 2\sigma_b^2. \tag{64}$$

The scattering function in (63), considered as a function of the frequency at any value of λ, is a one-pole spectrum centered at $f = -k_i(\lambda)/2\pi$ with a peak value $c^2\tilde{Q}(\lambda)/k_r^2(\lambda)$ and 3-db points $\pm k_r(\lambda)/2\pi$ about the center frequency.

In Fig. 13.6 we show the scattering function for the case when

$$\tilde{Q}(\lambda) = \begin{cases} 1 - \cos\left(\dfrac{2\pi\lambda}{L}\right), & 0 \leq \lambda \leq L, \\ 0, & \text{elsewhere,} \end{cases} \tag{65}$$

and

$$\tilde{k}(\lambda) = \begin{cases} k\left(1 - \tfrac{1}{2}\sin\left(\dfrac{\pi\lambda}{L}\right)\right), & 0 \leq \lambda \leq L, \\ 0, & \text{elsewhere.} \end{cases} \tag{66}$$

Except for the constraints of (58), (59), and (64), $\tilde{Q}(\lambda)$ and $k(\lambda)$ are arbitrary. This permits considerable flexibility in the choise of $\tilde{S}_{DR}\{f, \lambda\}$, even for this first-order model. For instance, if $k_i(\lambda)$ is proportional to λ, then $\tilde{S}_{DR}\{f, \lambda\}$ is sheared in the λ, f plane. We can choose $\tilde{Q}(\lambda)$ to give a multimodal (in λ) scattering function. In Fig. 13.7 we show a scattering function that exhibits both the multimodal behavior and the

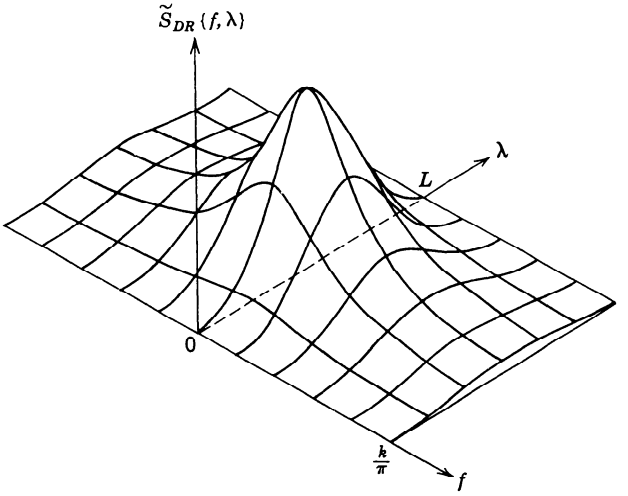

Fig. 13.6 Scattering function specified by (65) and (66) (from [7]).

shearing effect. Here

$$\tilde{Q}(\lambda) = \begin{cases} 1 - \cos\left(\dfrac{2\pi\lambda}{L}\right), & 0 \le \lambda \le \dfrac{L}{4}, \quad \dfrac{3L}{4} \le \lambda \le L, \\ 2 + \cos\left(\dfrac{\pi\lambda}{L}\right), & \dfrac{L}{4} \le \lambda \le \dfrac{3L}{4}, \\ 0, & \text{elsewhere,} \end{cases} \tag{67}$$

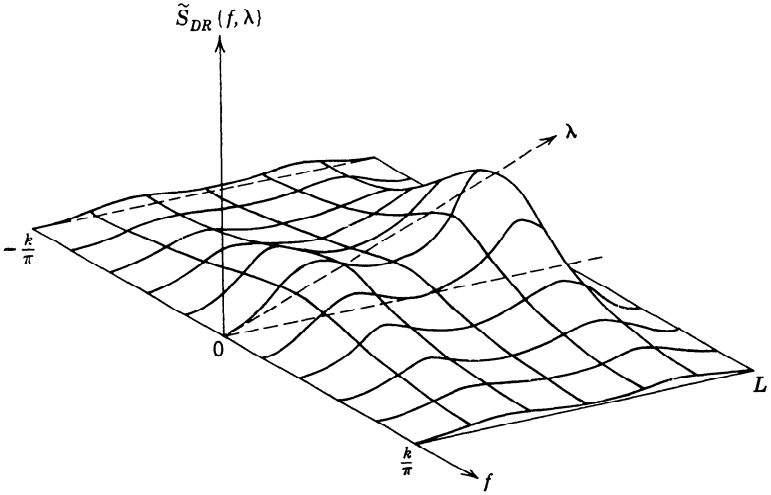

Fig. 13.7 Scattering function specified by (67) and (68) (from [7]).

and

$$\tilde{k}(\lambda) = k\left(1 - \frac{\lambda}{2L}\right) - j\left(\frac{3k\lambda}{5\pi L}\right). \tag{68}$$

This example illustrates the flexibility available with a first-order model. By using a higher-order system, we can describe any scattering function that is a rational function in f for each value of λ. To obtain multimodal behavior in f requires at least a second-order state model.

Just as in our previous work, the main advantage of the state-variable formulation is that it enables us to express the optimum receiver and its performance in a form such that we can actually compute an explicit answer. We shall look at specific examples of this model in Sections 13.2 and 13.3.

13.1.3 Model Summary

In this section we have developed a model for a doubly-spread target. The target return is characterized by either a scattering function or a distributed state-variable model.

In the next three sections we discuss various situations in which doubly-spread targets are the central issue. As we pointed out earlier, because the sections deal with different physical problems they can almost be read independently. (There are a few cross-references, but these can be understood out of context.)

13.2 DETECTION IN THE PRESENCE OF REVERBERATION OR CLUTTER (RESOLUTION IN A DENSE ENVIRONMENT)

In this section we consider the problem of detecting the return from a slowly fluctuating point target in the presence of distributed interference. The problem is an extension of our discrete resolution discussion in Section 10.5.

This type of problem is often encountered in active sonar systems. The complex envelope of the transmitted signal is $\sqrt{E_t}\tilde{f}(t)$. The target of interest is a slowly fluctuating point target that is located at a known delay τ_d and known Doppler ω_d. As the transmitted signal travels through the ocean, it encounters various inhomogeneities and numerous objects that cause reflections. A possible target environment is shown in Fig. 13.8. The return of the distributed interference is referred to as reverberation in the sonar case and as clutter in the radar case.

These reflections can be modeled as a spatial Poisson random process. In [1] we have developed the model in detail (see [2], [3] also). When there

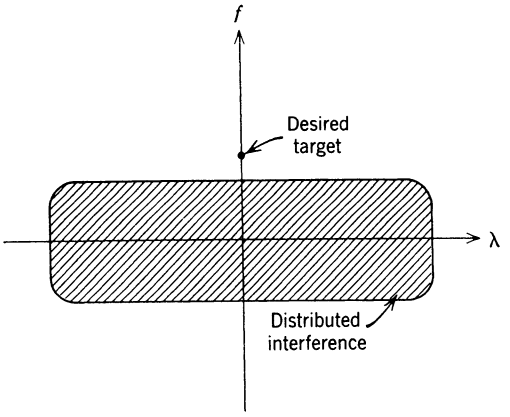

Fig. 13.8 Target environment in (λ, f) plane.

are a large number of reflectors we are led back to the complex Gaussian model of Section 13.1. There has been a great deal of work done on reverberation models, which the interested reader may consult (e.g., [8]–[18]). It appears that in many situations our spatial Poisson model is an adequate description of the environment.

Denoting the complex envelope of the reverberation return as $\tilde{n}_r(t)$, we have

$$\tilde{n}_r(t) = \sqrt{E_t}\int_{-\infty}^{\infty} \tilde{f}(t-\lambda)\tilde{b}\left(t-\frac{\lambda}{2}, \lambda\right) d\lambda. \tag{69}$$

This is a zero-mean complex Gaussian process with the covariance function

$$\tilde{K}_{\tilde{n}_r}(t, u) = E_t\int_{-\infty}^{\infty} \tilde{f}(t-\lambda)\tilde{K}_{DR}\{t-u, \lambda\}\tilde{f}^*(u-\lambda)\, d\lambda. \tag{70}$$

[These are just (2) and (5) repeated.] Alternatively, we can write (70) as

$$\tilde{K}_{\tilde{n}_r}(t, u) = E_t\int_{-\infty}^{\infty}\int \tilde{f}(t-\lambda)\tilde{S}_{DR}\{f, \lambda\}\tilde{f}^*(u-\lambda)e^{j2\pi f(t-u)}\, df\, d\lambda. \tag{71}$$

The function $\tilde{S}_{DR}\{f, \lambda\}$ is the scattering function of the reverberation and characterizes its distribution in range and Doppler. In addition to the reverberation return there is an additive, statistically independent complex white noise process $\tilde{w}(t)$. Thus, we have the following hypothesis testing problem:

$$\begin{aligned} \tilde{r}(t) &= \tilde{b}\tilde{f}(t-\tau_d)e^{j\omega_d t} + \tilde{n}_r(t) + \tilde{w}(t), && -\infty < t < \infty : H_1, \\ \tilde{r}(t) &= \tilde{n}_r(t) + \tilde{w}(t), && -\infty < t < \infty : H_0. \end{aligned} \tag{72}$$

This is just a detection in colored noise problem that we encountered previously in Section 9.2. The only new feature is the dependence of the colored noise covariance function on the transmitted signal. Notice that this problem is just the continuous version of the discrete resolution problem discussed in Section 10.5. Just as in that case, we can consider two types of receivers:

1. The *conventional receiver*, which is designed assuming that only white noise is present.
2. The *optimum receiver*, whose design is based on the assumed statistical knowledge of the reverberation.

In Section 13.2.1 we study the performance of the conventional receiver. In this case we try to eliminate the reverberation by choosing the signal properly. In Section 13.2.2 we study the optimum receiver problem. In this case we try to eliminate the reverberation by both signal design and receiver design.

13.2.1 Conventional Receiver

We consider the problem of detecting a target at some known delay τ_d and Doppler ω_d. If there were no reverberation, the results in Section 9.2 would be directly applicable. From (9.36), we compute

$$\tilde{l} \triangleq \int_{-\infty}^{\infty} \tilde{r}(t)\tilde{f}^*(t-\tau_d)e^{-j\omega_d t}\,dt. \tag{73}$$

The test consists of comparing $|\tilde{l}|^2$ with a threshold,

$$|\tilde{l}|^2 \underset{H_0}{\overset{H_1}{\gtrless}} \gamma. \tag{74}$$

When reverberation is present, this receiver is not optimum. It is frequently used for several reasons:

1. It is simpler than the optimum receiver.
2. The scattering function may not be known, and so we cannot design the optimum receiver.
3. Our analysis will demonstrate that it works almost as well as the optimum receiver in many situations.

It is straightforward to calculate the effect of the reverberation on the performance of the conventional receiver. The output $\tilde{l}$ is still a complex Gaussian random variable, so that Δ as defined in (9.49) is a complete

performance measure. The definition of Δ is

$$\Delta_{wo} \triangleq \frac{E\{|\tilde{l}|^2 \mid H_1\} - E\{|\tilde{l}|^2 \mid H_0\}}{E\{|\tilde{l}|^2 \mid H_0\}}. \tag{75}$$

As in Section 10.5, we use the subscript *wo* to denote that the receiver would be *optimum* in the presence of *white* noise only. Using (70), (72), and (73), we have

$$\begin{aligned}
&E\{|\tilde{l}|^2 \mid H_0\} \\
&= E\left\{\int_{-\infty}^{\infty} [\tilde{n}_r(t) + \tilde{w}(t)]\tilde{f}^*(t-\tau_d)e^{-j\omega_d t}\,dt \right. \\
&\quad \left. \times \int_{-\infty}^{\infty} [\tilde{n}_r^*(u) + \tilde{w}^*(u)]\tilde{f}(u-\tau_d)e^{j\omega_d u}\,du\right\} \\
&= \int_{-\infty}^{\infty} dt \int_{-\infty}^{\infty} du\, \tilde{f}^*(t-\tau_d)\tilde{f}(u-\tau_d)e^{-j\omega_d(t-u)} \\
&\quad \times \left[E_t \int_{-\infty}^{\infty} \tilde{f}(t-\lambda)\tilde{K}_{DR}(t-u,\lambda)\tilde{f}^*(u-\lambda)\,d\lambda + N_0\,\delta(t-u)\right].
\end{aligned} \tag{76}$$

Now recall that

$$\tilde{K}_{DR}(t-u,\lambda) = \int_{-\infty}^{\infty} \tilde{S}_{DR}\{f,\lambda\}e^{j2\pi f(t-u)}\,df. \tag{77}$$

Using (77) in (76) and rearranging terms, we obtain

$$\begin{aligned}
E\{|\tilde{l}|^2 \mid H_0\} = N_0 + E_t \int_{-\infty}^{\infty} df \int_{-\infty}^{\infty} d\lambda\, \tilde{S}_{DR}\{f,\lambda\} \\
\times \left[\int_{-\infty}^{\infty} dt\, \tilde{f}(t-\lambda)\tilde{f}^*(t-\tau_d)e^{j2\pi(f-f_d)t}\right] \\
\times \left[\int_{-\infty}^{\infty} du\, \tilde{f}^*(u-\lambda)\tilde{f}(u-\tau_d)e^{-j2\pi(f-f_d)u}\right].
\end{aligned} \tag{78}$$

The product of the quantities in the two brackets is just the signal ambiguity function, $\theta\{\tau_d - \lambda, f - f_d\}$. Thus,

$$E\{|\tilde{l}|^2 \mid H_0\} = N_0 + E_t \iint_{-\infty}^{\infty} df\, d\lambda\, \tilde{S}_{DR}\{f,\lambda\}\theta\{\tau_d - \lambda, f - f_d\}. \tag{79}$$

Thus, the effect of the reverberation is obtained by convolving the *reverberation scattering function* with the *signal ambiguity function*, $\theta\{\tau, -f\}$.† Similarly,

$$E[|\tilde{l}|^2 \mid H_1] = \bar{E}_r + E[|\tilde{l}|^2 \mid H_0], \tag{80}$$

† This result was first obtained by Steward and Westerfeld [19], [20].

so that

$$\Delta_{wo} = \frac{\bar{E}_r/N_0}{1 + E_t/N_0 \int_{-\infty}^{\infty}\int df\, d\lambda\, \tilde{S}_{DR}\{f, \lambda\}\theta\{\tau_d - \lambda, f - f_d\}}. \tag{81}$$

The second term in the denominator represents the degradation due to the reverberation,

$$\rho_r \triangleq \frac{E_t}{N_0} \int_{-\infty}^{\infty}\int df\, d\lambda\, \tilde{S}_{DR}\{f, \lambda\}\theta\{\tau_d - \lambda, f - f_d\}. \tag{82}$$

Using Property 4 given in (10.116), we can write ρ_r as

$$\rho_r = \frac{E_t}{N_0} \int_{-\infty}^{\infty}\int df\, d\lambda\, \tilde{S}_{DR}\{f, \lambda\}\theta\{\lambda - \tau_d, f_d - f\}. \tag{83}$$

We see that ρ_r increases as we increase the transmitted energy. This means that we cannot combat reverberation by simply increasing the transmitted energy. This result is not surprising, because the reverberation is caused by a reflection of the transmitted signal.

The result in (83) has the simple graphical interpretation shown in Fig. 13.9. We assume that transmitted signal has a Gaussian envelope and a linear frequency characteristic (see Example 4 on page 290)

$$\tilde{f}(t) = \left(\frac{1}{\pi T^2}\right)^{1/4} \exp\left[-\left(\frac{1}{2T^2} - jb\right)t^2\right]. \tag{84}$$

The equal-height contours of the ambiguity function are shown in Fig. 13.9*a*. The equal-height contours of the reverberation scattering function are shown in Fig. 13.9*b*. To evaluate ρ_r, we center $\theta\{\tau, -f\}$ at the desired target location (τ_d, f_d) as shown in Fig. 13.9*c*. The value of ρ_r will be determined by the amount of overlap of the two functions. For this particular target we can decrease the overlap in one of two ways:

1. Let $b = 0$ and make T large.
2. Let T be small and b any value.

These observations can be verified qualitatively by sketching the resulting functions. We shall verify them quantitatively later in the section.

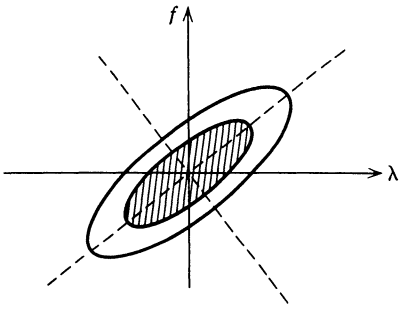

(a) Equal-height contours of $\theta(\tau, f)$

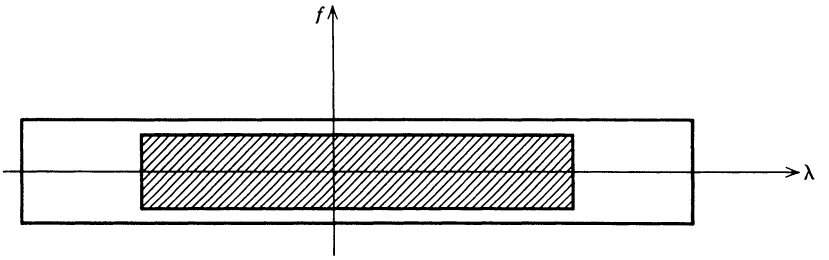

(b) Equal-height contours of $\tilde{S}_{DR}(f, \lambda)$

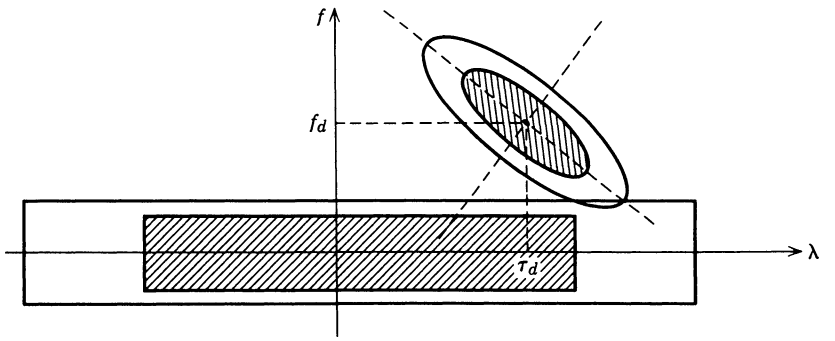

(c) Superposition

Fig. 13.9 Graphical interpretation of ρ_r integral.

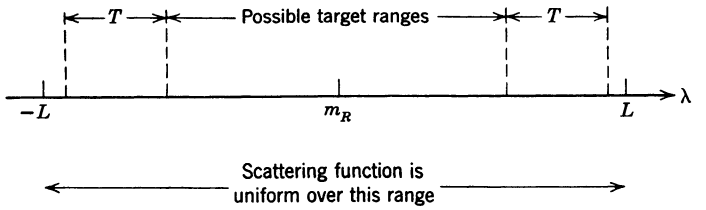

Fig. 13.10 Geometry for range-invariant approximation to the scattering function.

For future reference we observe that we also write ρ_r in terms of the two-frequency correlation function as

$$\rho_r = \frac{E_t}{N_0} \int_{-\infty}^{\infty} \int d\tau \, dv \, \tilde{R}_{DR}\{\tau, v\} \theta\{\tau, v\} \exp\left[-j2\pi(\tau f_d - v\tau_d)\right]. \tag{85}$$

The results in (83) and (85) are valid for an arbitrary scattering function. A special case of interest is when the scattering function is essentially infinite in length and has a uniform Doppler profile.

Range-Invariant Scattering Functions. When the scattering function has a uniform Doppler profile and extends beyond the range of a possible target by a distance greater than T, we can treat it as if it were infinite in extent. The geometry is shown in Fig. 13.10. We write

$$\tilde{S}_{DR}\{f, \lambda\} \triangleq \tilde{S}_{Du}\{f\}, \qquad -\infty < \lambda < \infty. \tag{86}$$

Notice that both sides of (86) have units $\text{cps}^{-1} \times \text{meter}^{-1}$. Thus,

$$E_t \int_{-\infty}^{\infty} \tilde{S}_{Du}\{f\} \, df \tag{87}$$

is the average received energy per meter of reverberation.

We can calculate ρ_r by specializing the result in (83). We can also calculate ρ_r directly from the original model. We carry out the second procedure because it has more intuitive appeal.

When the reverberation is infinite in extent, the reverberation return is a sample function of a stationary process. Using (86) in (71), we have

$$\tilde{K}_{\tilde{n}_r}(t, u) = E_t \tilde{K}_{Du}(t - u) \int_{-\infty}^{\infty} \tilde{f}(t - \lambda) \tilde{f}^*(u - \lambda) \, d\lambda. \tag{88}$$

The integral can be written as

$$\int_{-\infty}^{\infty} d\lambda \int_{-\infty}^{\infty} \tilde{F}\{f_1\} e^{j2\pi f_1(t-\lambda)} \, df_1 \int_{-\infty}^{\infty} \tilde{F}^*\{f_2\} e^{-j2\pi f_2(t-\lambda)} \, df_2$$

$$= \int_{-\infty}^{\infty} e^{j2\pi f_1(t-u)} \tilde{S}_{\tilde{f}}\{f_1\} \, df_1, \tag{89}$$

where

$$\tilde{S}_{\tilde{f}}\{f_1\} \triangleq |\tilde{F}\{f_1\}|^2. \tag{90}$$

Using (89) in (88) and transforming both sides, we obtain

$$\boxed{\tilde{S}_{\tilde{n}_r}\{f\} = E_t \tilde{S}_{Du}\{f\} \otimes \tilde{S}_{\tilde{f}}\{f\}.} \tag{91}$$

Thus the spectrum of the reverberation return is obtained by convolving the Doppler spectrum with the pulse spectrum. To compute the degradation for a stationary input process, we use (76) and (82) and obtain

$$\boxed{\rho_r = \frac{E_t}{N_0} \int_{-\infty}^{\infty} \tilde{S}_{\tilde{n}_r}\{f\} \tilde{S}_{\tilde{f}}\{f - f_d\}\, df.} \tag{92}$$

The results in (91) and (92) specify the degradation for this special case. A simple example illustrates the application of (92).

Example. We assume that the Doppler profile is Gaussian, so that $\tilde{S}_{Du}\{f\}$ is

$$\tilde{S}_{Du}\{f\} = \frac{N_r}{\sqrt{2\pi}\,\sigma_D} e^{-f^2/2\sigma_D^2}, \tag{93}$$

where σ_D is the root-mean-square Doppler spread in cycles per second. Assume that the signal is a pulse with a Gaussian envelope and linear FM sweep rate of $2b$ cps/sec. Thus $\tilde{f}(t)$ is

$$\tilde{f}(t) = \left(\frac{1}{\pi T^2}\right)^{1/4} \exp\left[-\left(\frac{1}{2T^2} - jb\right)t^2\right], \qquad -\infty < t < \infty. \tag{94}$$

Then

$$\tilde{S}_{\tilde{f}}\{f\} = \frac{1}{\sqrt{2\pi}\,B_f} e^{-f^2/2B_f^2}, \qquad -\infty < f < \infty, \tag{95}$$

where

$$B_f \triangleq \frac{(\overline{\omega^2})^{1/2}}{2\pi} = \frac{\sigma_w}{2\pi} = \frac{1}{2\pi}\left(\frac{1}{2T^2} + 2b^2T^2\right)^{1/2} \tag{96}$$

is the root-mean-square signal bandwidth in cycles per second [recall (10.48)].

Convolving (93) and (96) gives

$$\tilde{S}_{\tilde{n}_r}\{f\} = \frac{N_r E_t}{\sqrt{2\pi}\,\gamma} e^{-f^2/2\gamma^2}, \tag{97}$$

where

$$\gamma^2 \triangleq \sigma_R^2 + B_f^2. \tag{98}$$

Using (95) and (97) in (92), we have

$$\rho_r = \frac{E_t}{N_0} \frac{N_r}{2\pi\gamma B_f} \int_{-\infty}^{\infty} \exp\left(-\frac{(f - f_d)^2}{2B_f^2} - \frac{f^2}{2\gamma^2}\right) df. \tag{99a}$$

Integrating and rearranging terms gives

$$\rho_r = \frac{E_t N_r}{N_0 \sqrt{2\pi}\,\sigma_R} \frac{1}{\sqrt{1 + 2(B_f/\sigma_R)^2}} \exp\left[-\frac{1}{2}\frac{(f_d/\sigma_R)^2}{(1 + 2(B_f/\sigma_R)^2)}\right]. \tag{99b}$$

We see that the loss depends on the three quantities:

1. $D \triangleq \dfrac{E_t N_r}{N_0 \sqrt{2\pi}\,\sigma_R}$, the ratio of the reverberation power to the noise power in the equivalent rectangular bandwidth of the reverberation.
2. $\dfrac{f_d}{\sigma_R}$, the ratio of the target Doppler to the root-mean-square Doppler spread of the reverberation.
3. $\dfrac{B_f}{\sigma_R}$, the ratio of the effective signal bandwidth to the rms the Doppler spread of the reverberation.

The performance is given by substituting (99*b*) into (81) to obtain

$$\Delta_{wo,n} \triangleq \frac{\Delta_{wo}}{\bar{E}_r/N_0} = \frac{1}{1 + \rho_r}. \tag{100}$$

In Fig. 13.11, $\Delta_{wo,n}$ is plotted for some representative values of D.

D	Physical meaning	Figure
0.3	Reverberation < additive noise	13.11*a*
1.0	Reverberation = additive noise	13.11*b*
10.0	Reverberation/additive noise = 10 db	13.11*c*
100.0	Reverberation/additive noise = 20 db	13.11*d*

The parameters on the curves are f_d/σ_R. This is ratio of the target Doppler shift to the root-mean-square Doppler spread of the reverberation. The horizontal axis is B_f/σ_R. This is the ratio of the signal bandwidth to the root-mean-square Doppler spread of the reverberation. Two observations may be made with respect to this class of signals:

1. For zero target velocities, we have monotone improvement as the bandwidth increases.
2. For nonzero target velocities, one can use either very small or very large bandwidth signals.

The logic of these results follows easily from the diagrams shown in Figs. 13.12 and 13.13.

In Fig. 13.12, we show a zero-velocity target. As we increase the bandwidth, either by shortening the pulse (decreasing T) or by increasing the sweep rate (increasing b), the common volume between the ambiguity function and the reverberation decreases monotonically. In Fig. 13.13, we show a non-zero-velocity target. By transmitting a *long* pulse with no frequency modulation, the width of the ambiguity function in the Doppler direction is small and the common volume is negligible. If we shorten the pulse (by decreasing T) or widen the bandwidth (by increasing b), the result in Fig. 13.12*b* is obtained. We have increased the common volume, and the performance is degraded as shown in Fig. 13.10*c* and *d*. Finally, as B_f continues to increase, as shown in Fig. 13.12*c*, the width of the overlapping part of the ambiguity function decreases (it is $\simeq B_f^{-1}$), and the performance increases again.

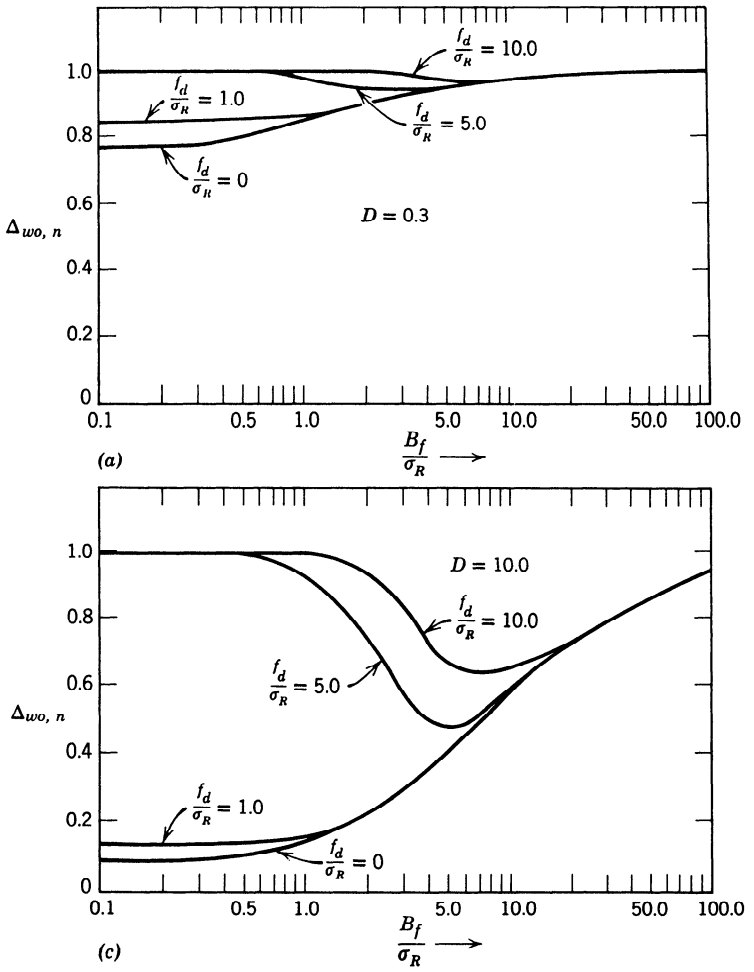

Fig. 13.11 Performance of conventional receiver in the presence of reverberation.

This example demonstrates the importance of matching the signal to the environment of interest. In this particular case, one might want to have two types of signals available: a long, unmodulated pulse, which is easy to generate and very effective for moving targets, and a linear FM pulse, which is effective for targets whose velocity was less than the root-mean-square Doppler spread. The example also illustrates an environment in which the signal design problem is relatively insensitive to detailed assumptions in the model. In other words, the basic results depend more on σ_R, the root-mean-square Doppler spread of the reverberation, than on the detailed shape of $\tilde{S}_{Du}\{f\}$.

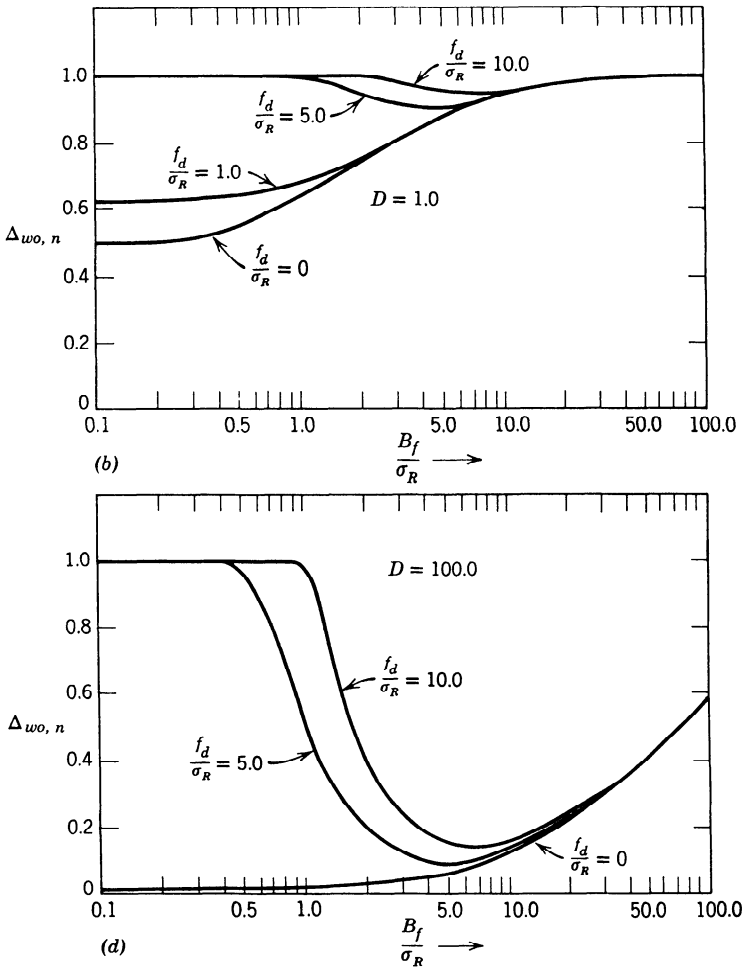

Fig. 13.11 (continued)

There are several comments with respect to the effect of reverberation on the performance that apply to both the range-invariant case and the general problem in which $\tilde{S}_{DR}\{f, \lambda\}$ is a function of λ.

1. The evaluation of receiver performance is always straightforward. At worst, a numerical evaluation of (83), (85), or (92) is required.
2. The problem of designing the optimum signal to minimize ρ_r subject to suitable constraints such as energy, bandwidth, or duration is mathematically difficult and can usually be avoided. Even if we could solve it,

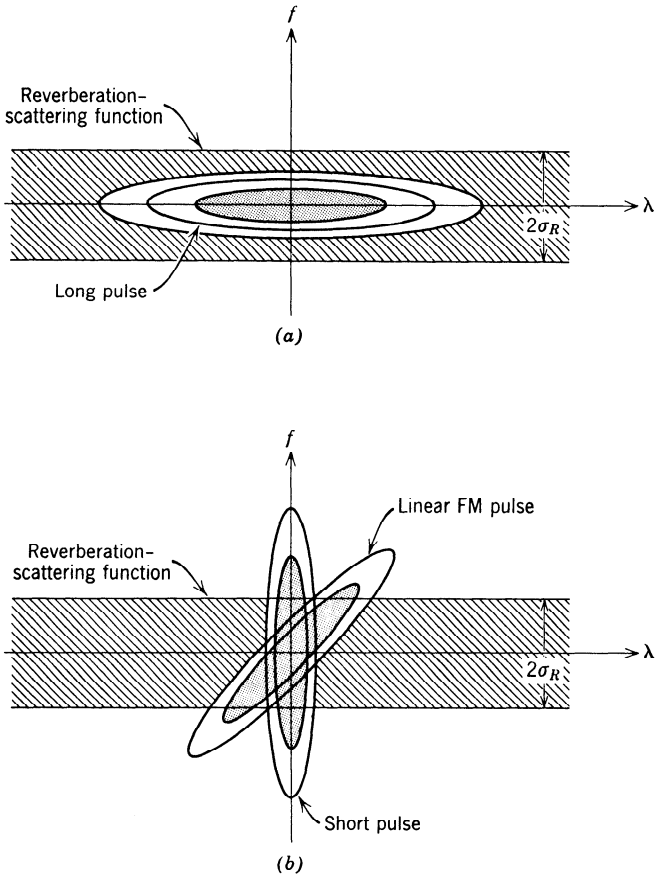

Fig. 13.12 Zero-velocity target in reverberation.

the solution would vary with $\tilde{S}_{DR}\{f, \lambda\}$, τ_d, and f_d. A more practical solution is the following:

(a) Choose a class of signals [e.g., the coded pulse sequence in (10.145)]. Maximize their performance by varying the parameters.

(b) Consider a set of allowable scattering functions instead of a specific scattering function. This gives a result that is less sensitive to the detailed environment.

There are a number of references dealing with the signal design problem at various levels of sophistication (e.g., [21]–[28]).

3. The nature of the ambiguity function of a sequence of pulses with complex weightings make it an excellent waveform for reverberation

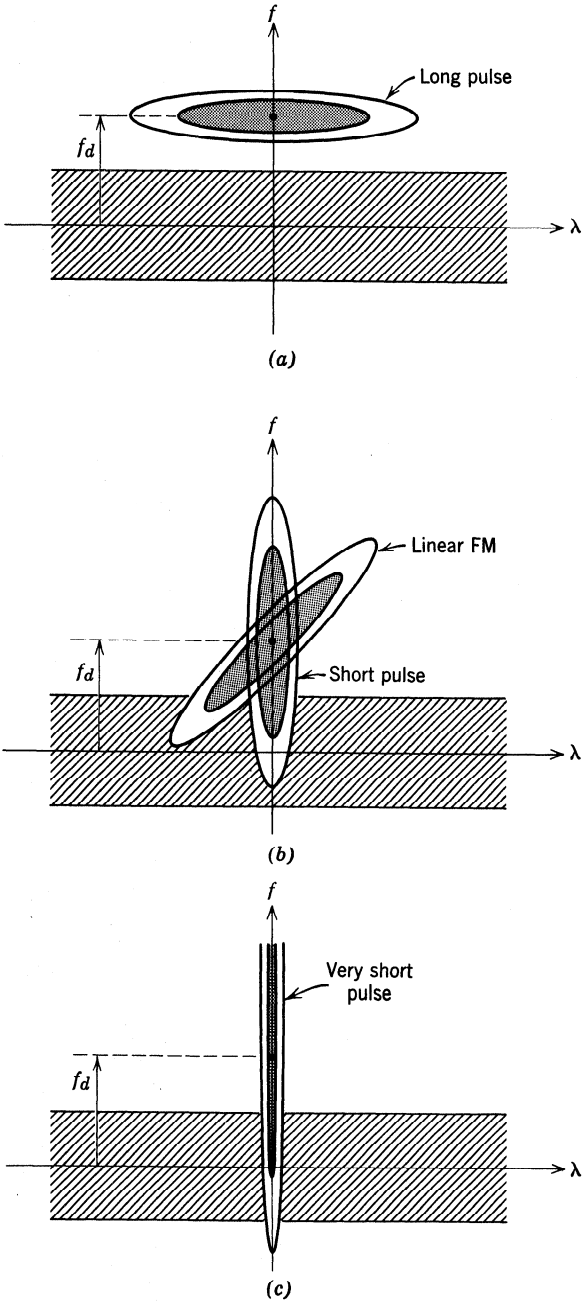

Fig. 13.13 Target with nonzero velocity in reverberation.

suppression. Because it is also easy to generate and detect, it is used in many systems.

This completes our discussion of the conventional receiver performance. We now turn to the optimum receiver problem.

13.2.2 Optimum Receivers

The problem of interest was given in (72), but we restate it here for convenience. The complex envelopes of the received waveforms on the two hypotheses are

$$\tilde{r}(t) = \tilde{b}\tilde{f}_d(t) + \tilde{n}_r(t) + \tilde{w}(t), \qquad -\infty < t < \infty : H_1 \tag{101}$$

and

$$\tilde{r}(t) = \tilde{n}_r(t) + \tilde{w}(t), \qquad -\infty < t < \infty : H_0, \tag{102}$$

where

$$\tilde{f}_d(t) \triangleq \tilde{f}(t - \tau_d)e^{j\omega_d t}. \tag{103}$$

The reverberation return is a sample function of a complex Gaussian random process whose covariance function is given by (70) as

$$\tilde{K}_{\tilde{n}_r}(t, u) = E_t \int_{-\infty}^{\infty} \tilde{f}(t - \lambda)\tilde{K}_{DR}(t - u, \lambda)\tilde{f}^*(u - \lambda)\, d\lambda. \tag{104}$$

We want to find the optimum receiver to detect $\tilde{f}_d(t)$. This is just the familiar problem of detecting a slowly fluctuating point target in the presence of nonwhite Gaussian noise, which we solved in Section 9.3.

The optimum receiver computes

$$\tilde{l} \triangleq \int_{-\infty}^{\infty} \tilde{g}^*(t)\tilde{r}(t)\, dt, \tag{105}$$

where $\tilde{g}(\cdot)$ satisfies

$$\tilde{f}_d(t) = \int_{-\infty}^{\infty} \tilde{K}_{\tilde{n}_r}(t, u)\tilde{g}(u)\, du + N_0\tilde{g}(t), \qquad -\infty < t < \infty. \tag{106}$$

It then compares $|\tilde{l}|^2$ with a threshold. Using (104) in (106) gives the equation we must solve to find the optimum receiver. It is

$$\tilde{f}_d(t) = E_t \int\int_{-\infty}^{\infty} \tilde{f}(t - \lambda)\tilde{K}_{DR}(t - u, \lambda)\tilde{f}^*(u - \lambda)\tilde{g}(u)\, du\, d\lambda + N_0\tilde{g}(t), \qquad -\infty < t < \infty. \tag{107}$$

For arbitrary $\tilde{K}_{DR}(\cdot, \cdot)$ the solution of (107) is difficult. There are several cases when a solution can be obtained.

Case 1. If the functions $\tilde{f}(t)$ and $\tilde{K}_{DR}(t-u, \lambda)$ are of a form so that the eigenvalues and eigenfunctions of (104) can be found, the solution to (107) follows easily. One example of this is the discrete resolution problem of Section 10.5. A second example is when $\tilde{K}_{DR}(t-u, \lambda)$ is a separable kernel. A third example is when $\tilde{f}(t)$ is a Gaussian pulse and $\tilde{K}_{DR}(t-u, \lambda)$ is doubly Gaussian. The basic procedure in this case is familiar, and so we relegate it to the problems.

Case 2. If we can describe the channel-scattering function by the distributed differential-equation model of Section 13.1.2, we can find the optimum receiver. We discuss this case in detail in the next subsection.

Case 3. If the scattering function is long in the λ-dimension (as shown in Fig. 13.10) and has a uniform Doppler profile, then $\tilde{n}_r(t)$ is a stationary process and (107) can be solved using Fourier transforms. We studied the conventional receiver for this case on page 466. On page 477, we study the optimum receiver and compare the performance of the two systems.

We now carry out the analysis of Cases 2 and 3.

Case 2. Optimum Receiver: State-Variable Realization. In Section 9.4, we developed a realization of the optimum receiver for the detection of a slowly fluctuating target in nonwhite noise. This realization was based on a realizable whitening filter and contained the minimum mean-square error estimate of the nonwhite noise as a basic component. This realization of the optimum receiver is shown in Fig. 13.14 (this is just Fig. 9.8 with modified notation). The test statistic is

$$l_o = \left| \int_{T_i}^{T_f} dt \left[\int_{T_i}^{t} \tilde{h}_{wr}(t, z) \tilde{r}(z)\, dz \int_{T_i}^{t} \tilde{h}_{wr}^*(t, y) \tilde{f}_d^*(y)\, dy \right] \right|^2, \tag{108}$$

where $\tilde{h}_{wr}(t, z)$ is defined as

$$\tilde{h}_{wr}(t, z) \triangleq \left(\frac{1}{N_0} \right)^{1/2} \{ \delta(t-z) - \tilde{h}_{or}(t, z) \}. \tag{109}$$

The filter $\tilde{h}_{or}(t, z)$ is the optimum realizable filter for estimating $\tilde{n}_r(t)$ when the input is

$$\tilde{n}(t) = \tilde{n}_r(t) + \tilde{w}(t). \tag{110}$$

From (9.111) we have the degradation due to the colored noise,

$$\Delta_{dg} = \int_{T_i}^{T_f} [2\tilde{f}_d^*(t)\tilde{f}_r(t) - |\tilde{f}_r(t)|^2]\, dt. \tag{111}$$

The function $\tilde{f}_r(t)$ is the output of $\tilde{h}_{wr}(t, z)$ when the input is $\tilde{f}_d(t)$.

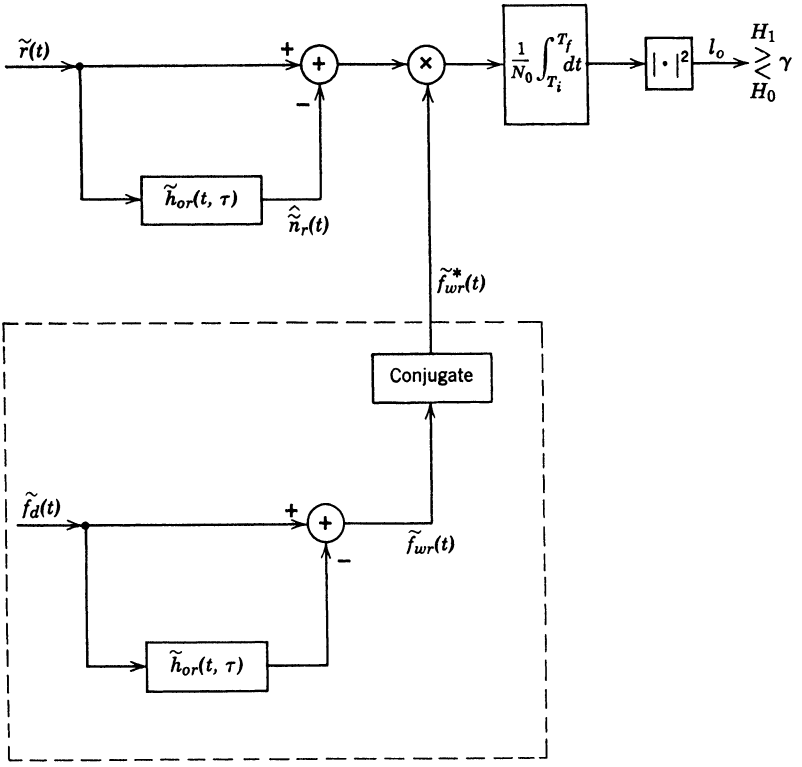

Fig. 13.14 Optimum receiver

We see that we can completely design the optimum receiver and analyze the receiver performance if we can find $\tilde{h}_{or}(t, z)$. In this section we derive a set of differential equations that specify $\hat{\tilde{n}}_r(t)$ [and therefore $\tilde{h}_{or}(t, z)$]. Our derivation is based on the distributed state-variable model in Section 13.1.2.

The differential equations describing $\tilde{n}_r(t)$ are analogous to (38)–(41). The state equation is

$$\frac{\partial \tilde{\mathbf{x}}(\lambda, t)}{\partial t} = \tilde{\mathbf{F}}(\lambda)\tilde{\mathbf{x}}(t, \lambda) + \tilde{\mathbf{G}}(\lambda)\tilde{u}(t, \lambda), \qquad t > T_i, \lambda \in \Omega_L, \tag{112}$$

where Ω_L is the range of λ where the target-scattering function is nonzero. The covariance function of $\tilde{u}(t, \lambda)$ is

$$E[\tilde{u}(t, \lambda)\tilde{u}^*(\tau, \lambda')] = \tilde{Q}(\lambda)\delta(t - \tau)\,\delta(\lambda - \lambda'). \tag{113}$$

The reverberation process is

$$\tilde{b}(t, \lambda) = \tilde{\mathbf{C}}(\lambda)\tilde{\mathbf{x}}(t, \lambda). \tag{114}$$

The colored noise due to the reverberation is

$$\tilde{n}_r(t) = \int_{-\infty}^{\infty} \sqrt{E_t}\tilde{f}(t-\lambda)\tilde{b}(t,\lambda)\,d\lambda$$

$$\triangleq \tilde{C}(t:\tilde{\mathbf{x}}(t,\lambda)), \tag{115}$$

which we refer to as the *modulation functional.*

The minimum mean-square error estimate is obtained by extending Kalman-Bucy filtering theory to include the spatial integral operator in (115). This extension was done originally by Tzafestas and Nightingale [29], [30]. The results are given in (116–121).†

The estimator equation is

$$\boxed{\frac{\partial\hat{\tilde{\mathbf{x}}}(t,\lambda)}{\partial t} = \tilde{\mathbf{F}}(\lambda)\hat{\tilde{\mathbf{x}}}(t,\lambda) + \tilde{\mathbf{z}}(t,\lambda)[\tilde{r}(t) - \tilde{C}(t:\hat{\tilde{\mathbf{x}}}(t,\lambda))], \quad t \geq T_i,\ \lambda \in \Omega_L.} \tag{116}$$

$$\hat{\tilde{\mathbf{x}}}(T_i,\lambda) = \mathbf{0}, \qquad \lambda \in \Omega_L. \tag{117}$$

The gain equation is

$$\boxed{\tilde{\mathbf{z}}(t,\lambda) = \frac{1}{N_0}\int_{\Omega_L} \tilde{\boldsymbol{\xi}}(t:\lambda,\lambda')\tilde{\mathbf{C}}^{\dagger}(\lambda')\sqrt{E_t}\tilde{f}^{*}(t-\lambda')\,d\lambda'.} \tag{118}$$

The function $\tilde{\boldsymbol{\xi}}(t:\lambda,\lambda')$ is the error covariance matrix

$$\tilde{\boldsymbol{\xi}}(t:\lambda,\lambda') \triangleq E[(\tilde{\mathbf{x}}(t,\lambda) - \hat{\tilde{\mathbf{x}}}(t,\lambda))(\tilde{\mathbf{x}}^{\dagger}(t,\lambda') - \hat{\tilde{\mathbf{x}}}^{\dagger}(t,\lambda'))]. \tag{119a}$$

Notice that

$$\tilde{\boldsymbol{\xi}}^{\dagger}(t:\lambda,\lambda') = \tilde{\boldsymbol{\xi}}(t:\lambda',\lambda). \tag{119b}$$

The covariance matrix satisfies the differential equation

$$\frac{\partial\tilde{\boldsymbol{\xi}}(t:\lambda,\lambda')}{\partial t} = \tilde{\mathbf{F}}(\lambda)\tilde{\boldsymbol{\xi}}(t:\lambda,\lambda') + \tilde{\boldsymbol{\xi}}(t:\lambda',\lambda)\tilde{\mathbf{F}}^{\dagger}(\lambda') + \tilde{\mathbf{G}}(\lambda)\tilde{Q}(\lambda)\tilde{\mathbf{G}}^{\dagger}(\lambda')\,\delta(\lambda-\lambda') - \tilde{\mathbf{z}}(t,\lambda)N_0\tilde{\mathbf{z}}^{\dagger}(t,\lambda'),$$

$$\lambda, \lambda' \in \Omega_L,\ t \geq T_i. \tag{120}$$

† We have omitted the derivation because, for the particular case described by (112)–(115), the reader should be able to verify that the result is correct (see Problem 13.2.15). The model studied in [29] is much more general than we need. The reader should note the similarity between (116)–(121) and the Kalman-Bucy equations of Section I-6.3. Other references dealing with estimation in distributed parameter systems include [70]–[75].

The reader should notice the similarity between (120) and (A.161). Using (118) in (120) gives

$$\frac{\partial \tilde{\xi}(t:\lambda,\lambda')}{\partial t} = \tilde{\mathbf{F}}(\lambda)\tilde{\xi}(t:\lambda,\lambda') + \tilde{\xi}(t:\lambda',\lambda)\tilde{\mathbf{F}}^{\dagger}(\lambda') + \tilde{\mathbf{G}}(\lambda)\tilde{Q}(\lambda)\tilde{\mathbf{G}}^{\dagger}(\lambda)\,\delta(\lambda-\lambda') - \frac{E_t}{N_0}\Big\{\int_{\Omega_L}\tilde{\xi}(t:\lambda,\sigma)\tilde{\mathbf{C}}^{\dagger}(\sigma)\tilde{f}^{*}(t-\sigma)\,d\sigma \times \int_{\Omega_L}\tilde{f}(t-\sigma')\tilde{\mathbf{C}}(\sigma')\tilde{\xi}(t:\sigma',\lambda')\,d\sigma'\Big\}, \quad \lambda,\lambda' \in \Omega_L,\ t \geq T_i. \tag{121a}$$

The initial condition is

$$\tilde{\xi}(T_i:\lambda,\lambda') = \tilde{\xi}_0(T_i,\lambda)\,\delta(\lambda-\lambda'). \tag{121b}$$

These equations completely specify the filter whose impulse response is $\tilde{h}_{or}(t,z)$. Thus, the receiver is completely specified and its performance can be calculated. The block diagram of the optimum estimator is shown in Fig. 13.15 (the heavy lines represent signals that are functions of both space and time). Using the system in Fig. 13.15 in the diagram of Fig. 13.14 gives the optimum receiver.

Several comments regarding the optimum receiver and the corresponding equations are useful.

1. The optimum filter contains spatial operations. In most cases these will be difficult to implement exactly. We discuss several approximate realizations in Section 13.3.
2. The performance of the optimum receiver provides a bound on the performance of simpler systems. To evaluate the performance we must find Δ_{dg} as specified in (111). This requires solving the variance equation (120).
3. The equations are algebraically complex. We shall find that we can obtain solutions to them with a reasonable amount of calculation.

We shall defer doing an example to illustrate the solution techniques until Section 13.3. The same filtering problem arises in that section, when we communicate over doubly-spread channels.

This concludes our discussion of the state-variable realization of the optimum receiver in the presence of reverberation. We now consider the third case listed in the introduction on page 473.

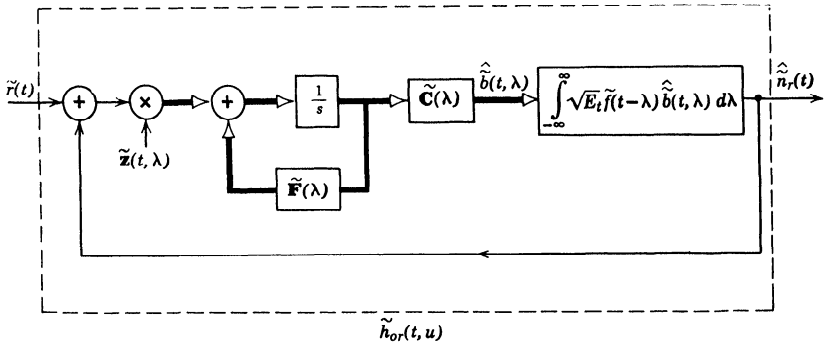

Fig. 13.15 Distributed state-variable realization of optimum realizable filter.

Case 3. Reverberation with Constant Doppler Profile and Infinite Range. In some cases Ω_L is long enough compared to the observation time that we can assume it is infinite (see Fig. 13.10). If, in addition,

$$\tilde{K}_{DR}(t-u,\lambda) = \tilde{K}_{Du}(t-u), \tag{122}$$

we can obtain a solution to (106) by using Fourier transform techniques. Using (122) in (104), we obtain

$$\tilde{K}_{\tilde{n}_r}(t,u) = E_t\tilde{K}_{Du}(t-u)\int_{-\infty}^{\infty}\tilde{f}(t-\lambda)\tilde{f}^*(u-\lambda)\,d\lambda, \tag{123}$$

which is identical with (88). From (91),

$$\tilde{S}_{\tilde{n}_r}\{f\} = E_t\tilde{S}_{Du}\{f\} \otimes \tilde{S}_{\tilde{f}}\{f\}, \tag{124}$$

where

$$\tilde{S}_{\tilde{f}}\{f\} \triangleq |\tilde{F}\{f\}|^2. \tag{125}$$

Using (124) in (106), transforming, and solving for $\tilde{G}_\infty\{f\}$ gives

$$\boxed{\tilde{G}_\infty\{f\} = \frac{\tilde{F}\{f-f_d\}}{N_0 + E_t\tilde{S}_{Du}\{f\} \otimes \tilde{S}_{\tilde{f}}\{f\}},} \tag{126a}$$

where f_d is Doppler shift of the desired target. For a zero-velocity target,

$$\boxed{G_\infty\{f\} = \frac{\tilde{F}\{f\}}{N_0 + E_t\tilde{S}_{Du}\{f\} \otimes \tilde{S}_{\tilde{f}}\{f\}}.} \tag{126b}$$

The performance is obtained from (9.77) as

$$\boxed{\Delta_o = \bar{E}_r\int_{-\infty}^{\infty}\frac{|\tilde{F}\{f-f_d\}|^2}{N_0 + \tilde{S}_{\tilde{n}_r}\{f\}}\,df.} \tag{127}$$

We now discuss a particular problem to illustrate the application of these results.

Example 1. We consider the same model as in the conventional receiver example on page 466. The signal is specified by (94), and the Doppler profile is given in (93). Using (95) and (97) in (127) gives

$$\Delta_o = \frac{\bar{E}_r}{N_0} \int_{-\infty}^{\infty} \frac{(\sqrt{2\pi}\, B_f)^{-1} e^{-(f-f_d)^2/2B_f^2}}{1 + (N_r E_t/\sqrt{2\pi}\, N_0 \gamma) e^{-f^2/2\gamma^2}}\, df. \tag{128}$$

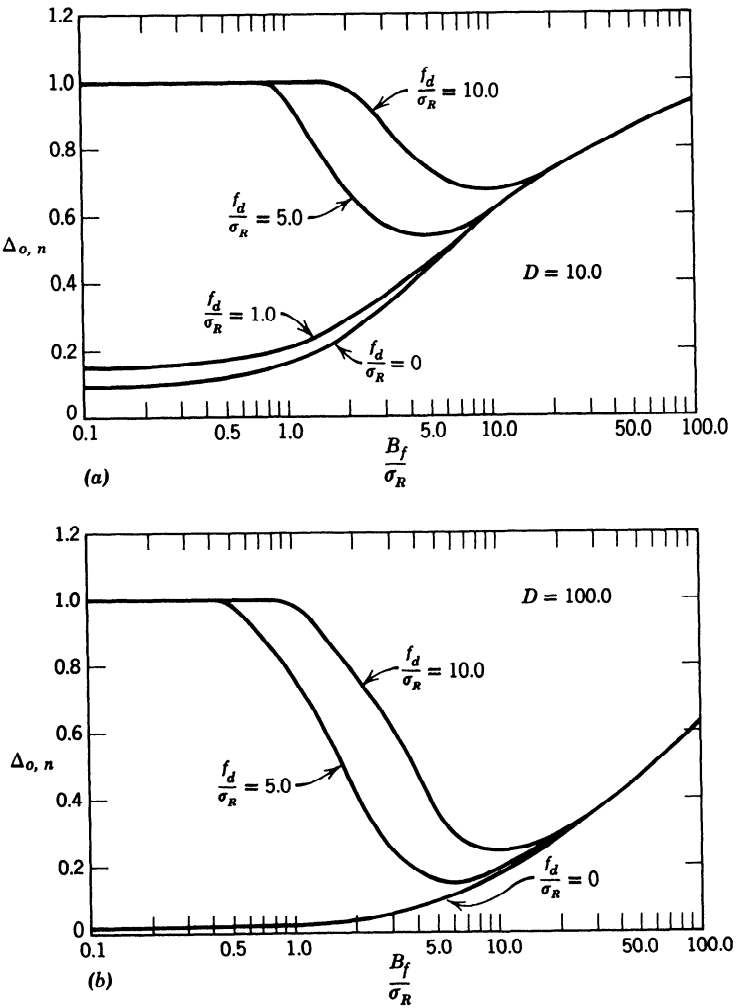

Fig. 13.16 Performance of optimum receiver in the presence of reverberation.

As in the conventional receiver case, the performance depends on $D, f_d/\sigma_R$, and B_f/σ_R, which were defined on page 467. When $D = 0.3$ and 1.0, the performances of the optimum receiver and the conventional receiver are almost the same. In Fig. 13.16, we have plotted $\Delta_o/(\bar{E}_r/N_0)$ for $D = 10$ and 100.

It is useful to consider a particular set of values. We assume the following set of parameter values:

$$\begin{aligned} f_d/\sigma_R &= 5.0, \\ B_f/\sigma_R &= 1.0, \\ D &= 100.0. \end{aligned} \tag{129}$$

We see that this set of parameters puts us in the valley on both curves (Figs. 13.16 and 13.11) and corresponds to a poor signal choice.

For this set of parameter values,

$$\Delta_o = 0.762 \frac{\bar{E}_r}{N_0} \tag{130}$$

and

$$\Delta_{wo} = 0.528 \frac{\bar{E}_r}{N_0}. \tag{131}$$

We see that, for a very poor signal choice, the difference is about 1.5 db. For any reasonably good signal choices, the difference in the performance of the two receivers is negligible. This is because a good signal choice decreases the reverberation return to a point where the optimum receiver is not needed.

We consider a second example briefly.

Example 2. In some cases, the Doppler spreading of the reverberation (or clutter) is small compared to the bandwidth of the signal energy spectrum, $\tilde{S}_{\tilde{f}}\{f\}$. In these cases it is convenient to approximate $\tilde{S}_{Du}\{f\}$ by an impulse,

$$\tilde{S}_{Du}\{f\} \simeq P_c\, \delta\{f\}. \tag{132}$$

We assume that $f_d = 0$, because a zero-velocity target is the most difficult to detect. Using (132) in (126*b*) gives

$$\tilde{G}_\infty\{f\} = \frac{\tilde{F}\{f\}}{N_0 + E_t P_c |\tilde{F}\{f\}|^2}. \tag{133}$$

For small values of reverberation return, such that

$$\frac{E_t P_c \tilde{S}_{\tilde{f}}\{f\}}{N_0} \ll 1, \tag{134}$$

we see that the optimum filter reduces to a matched filter. However, for large values of reverberation return,

$$\tilde{G}_\infty\{f\} \simeq \frac{1}{E_t P_c \tilde{F}^*\{f\}}, \tag{135}$$

which is an *inverse filter* (this filter was first derived in [31]). Thus, we see that the optimum receiver has an appreciably different character in the frequency ranges where reverberation rather than the additive white noise is the limiting factor.

To evaluate the performance, we use (132) in (127) and obtain

$$\Delta_o = \bar{E}_r \int_{-\infty}^{\infty} \frac{|\tilde{F}\{f\}|^2}{N_0 + E_t P_c |\tilde{F}\{f\}|^2}\, df. \tag{136}$$

It is useful to evaluate Δ_o for a particular signal set. We consider the Butterworth family whose energy spectrum is

$$\tilde{S}_{\tilde{f}}\{f\} = \frac{(2n/k)\sin(\pi/2n)}{(2\pi f/k)^{2n} + 1}, \qquad -\infty < f < \infty, \quad n = 1, 2, \ldots. \tag{137}$$

Substituting (137) into (136) and integrating gives

$$\Delta_o(n) = \frac{\bar{E}_r}{N_0}\left[1 + \frac{\pi E_t P_c}{kN_0}\frac{2n}{\pi}\sin\left(\frac{\pi}{2n}\right)\right]^{1/2n-1}. \tag{138a}$$

For $n = \infty$,

$$\Delta_o(\infty) = \frac{\bar{E}_r}{N_0}\left[1 + \frac{\pi E_t P_c}{kN_0}\right]^{-1}. \tag{138b}$$

Two conclusions follow from (138):

1. Increasing the energy in the transmitted signal is an ineffective way to combat reverberation; we see that, for strong reverberation,

$$\Delta_o(n) \propto E_t^{1/2n} \leq E_t^{1/2} \qquad \text{for} \quad E_t \geq 1, \tag{138c}$$

where we obtain equality by using an exponential pulse ($n = 1$).

2. As we would expect, Δ_o increases monotonically with k. (Recall Fig. 13.13.)

Notice that this example has considered a zero-velocity target, which is the most difficult to detect in the reverberation environment specified by (132). The performance increases monotonically with target velocity.

This case completes our discussion of the design and performance of optimum receivers in the presence of reverberation. We now summarize our discussion of the reverberation problem.

13.2.3 Summary of the Reverberation Problem

We have investigated the problem of signal and receiver design when the target is a slowly fluctuating point target and the interference consists of reflectors that are spread in range and Doppler and additive white noise. A number of interesting results were obtained.

1. If a conventional matched filter receiver is used, the degradation due to reverberation is

$$\rho_r = \frac{E_t}{N_0}\int_{-\infty}^{\infty}\int df\, d\lambda\, \tilde{S}_{DR}\{f, \lambda\}\theta\{\lambda - \tau_d, f_d - f\}. \tag{139}$$

This integral has the simple graphical interpretation shown in Fig. 13.9.

2. The optimal signal design problem for the conventional receiver consists of trying to minimize the common volume of the reverberation-scattering function and the shifted signal ambiguity function. The best signal will depend on the target's location in the range-Doppler plane as well as on $\tilde{S}_{DR}\{f, \lambda\}$.

3. If one can make the two functions essentially disjoint, the conventional and optimum receivers are identical and the performance is limited only by the additive noise.

4. If one is constrained to use a signal that results in an appreciable overlap, the optimum receiver provides an improved performance. It is important to remember that this improved performance requires a more complex receiver and assumes knowledge of the scattering function (including its level) and the additive noise level.

5. For a large number of cases we can find the optimum receiver and evaluate its performance. The techniques for performing this analysis were developed in detail.

We have confined our discussion to conventional and optimum receivers. A third category of receivers is useful in some situations. This receiver computes

$$l_m \triangleq \int_{-\infty}^{\infty} \tilde{r}(t)\tilde{v}^*(t)\, dt \tag{140}$$

and compares $|l_m|^2$ with a threshold. The function $\tilde{v}(t)$ is not necessarily the desired signal, $\tilde{f}_d(t)$, or the optimum correlation function $\tilde{g}(t)$ specified by (106). We might choose a $\tilde{v}(t)$ that is simpler to implement than $\tilde{g}(t)$ but performs better than $\tilde{f}_d(t)$. The performance of the receiver in (140) is given by

$$\Delta_m = \frac{\bar{E}_r \theta_{fv}\{\tau_d, f_d\}}{N_0\left[1 + E_t/N_0 \int_{-\infty}^{\infty}\int \tilde{S}_{DR}\{f, \lambda\}\theta_{fv}\{\lambda, -f\}\, df\, d\lambda\right]}, \tag{141}$$

where $\theta_{fv}\{\cdot, \cdot\}$ is the cross-ambiguity function defined in (10.222). We can now choose $\tilde{v}(t)$ to minimize Δ_m. Notice that we must put additional constraints on $\tilde{v}(t)$, or we shall find that the optimum $\tilde{v}(t)$ equals $\tilde{g}(t)$. One possible constraint is to require $\tilde{v}(t)$ to be a piecewise constant function. This would be a logical constraint if $\tilde{f}(t)$ were a sequence of rectangular pulses. Various other constraints are possible.

This particular formulation is attractive because it allows us to design a system that works better than the conventional receiver but can be constrained to be less complicated than the optimum receiver. This problem